NASA TECHNICAL MEMORANDUM

NASA TM X-3026

NASA TM X-3026

COMPARISON OF THEORETICAL AND EXPERIMENTAL BOUNDARY-LAYER DEVELOPMENT IN A MACH 2.5 MIXED-COMPRESSION INLET

by Warren R. Hingst and Charles E. Towne

Lewis Research Center
Cleveland, Ohio 44135

NATIONAL AERONAUTICS AND SPACE ADMINISTRATION • WASHINGTON, D. C. • APRIL 1974

1. Report No. NASA TM X-3026	2. Government Accession No.	3. Recipient's Catalog No.
4. Title and Subtitle COMPARISON OF THEORETICAL AND EXPERIMENTAL BOUNDARY-LAYER DEVELOPMENT IN A MACH 2.5 MIXED-COMPRESSION INLET		5. Report Date APRIL 1974 6. Performing Organization Code
7. Author(s) Warren R. Hingst and Charles E. Towne		8. Performing Organization Report No. E-7586 10. Work Unit No. 501-24
9. Performing Organization Name and Address Lewis Research Center, National Aeronautics and Space Administration, Cleveland, Ohio 44135		11. Contract or Grant No. 13. Type of Report and Period Covered Technical Memorandum
12. Sponsoring Agency Name and Address National Aeronautics and Space Administration, Washington, D.C. 20546		14. Sponsoring Agency Code

15. Supplementary Notes

16. Abstract

An analytical investigation was made of the boundary-layer flow in an axisymmetric Mach 2.5 mixed-compression inlet, and the results were compared with experimental measurements. The inlet tests were conducted in the Lewis 10- by 10-foot supersonic wind tunnel at a unit Reynolds number of 8.2×10^6/m The inlet incorporated porous bleed regions for boundary-layer control, and the effect of this bleed was taken into account in the analysis. The experimental boundary-layer data were analyzed by using similarity laws from which the skin-friction coefficient was obtained. The boundary-layer analysis included predictions of laminar and turbulent boundary-layer growth, transition, and the effects of the shock - boundary-layer interactions. In addition, the surface static pressures were compared with those obtained from an inviscid characteristics program The results of the investigation showed that the analytical techniques gave satisfactory predictions of the boundary-layer flow except in regions that were badly distorted by the terminal shock.

17. Key Words (Suggested by Author(s))	18. Distribution Statement
Boundary layers; Boundary-layer bleed; Shock - boundary-layer interaction; Boundary-layer analysis; Supersonic inlet; Mixed-compression inlet	Unclassified - unlimited Category 12 CAT. 12

19. Security Classif. (of this report)	20. Security Classif. (of this page)	21. No. of Pages	22. Price*
Unclassified	Unclassified	30	$3.25

* For sale by the National Technical Information Service Springfield, Virginia 22151

COMPARISON OF THEORETICAL AND EXPERIMENTAL BOUNDARY-LAYER DEVELOPMENT IN A MACH 2.5 MIXED-COMPRESSION INLET

by Warren R. Hingst and Charles E. Towne

Lewis Research Center

SUMMARY

An analytical investigation was made of the boundary-layer flow in an axisymmetric Mach 2.5 mixed-compression inlet, and the results were compared with experimental measurements. The inlet tests were conducted in the Lewis 10- by 10-foot supersonic wind tunnel at a unit Reynolds number of 8.2×10^6 per meter. The inlet incorporated porous bleed regions for boundary-layer control, and the effect of this bleed was taken into account in the analysis. The experimental boundary-layer data were analyzed by using similarity laws from which the skin-friction coefficient was obtained. The boundary-layer analysis included predictions of laminar and turbulent boundary-layer growth, transition, and the effects of the shock - boundary-layer interactions. In addition, the surface static pressures were compared with those obtained from an inviscid characteristics program. The results of the investigation showed that the analytical techniques gave satisfactory predictions of the boundary-layer flow except in regions that were badly distorted by the terminal shock.

INTRODUCTION

Analytical techniques have been used to predict viscous boundary-layer phenomena in supersonic inlets, as reported in references 1 and 2. The need for accurate methods to analyze these viscous effects is apparent if the alternative is considered, that is, extensive testing. A complete inlet test program to determine the viscous effects would require measurement of boundary-layer parameters, investigation of the shock - boundary-layer interaction, and determination of the amount and location of bleed used for boundary-layer control. In addition to these extensive test requirements, further difficulties arise because most testing is done with scale models at Reynolds numbers that differ from those encountered in flight. This introduces uncertainties when the test

results are applied to full-scale flight components. Therefore, accurate methods of predicting boundary-layer phenomena are essential in planning more efficient testing as well as in the application of these test results to flight conditions.

The primary purpose of this investigation was to compare the results of various analytical techniques with boundary-layer measurements taken in a Mach 2.5 axisymmetric, mixed-compression inlet. The inlet had a 60-percent internal-area contraction at the design operating condition and incorporated bleed systems for boundary-layer control. The measurements made in the inlet tests included surface static pressures, bleed flow rates, and boundary-layer profiles upstream and downstream of the shock - boundary-layer interactions. The experimental results of the inlet tests were initially reported in reference 3.

The inlet internal surface static-pressure measurements were compared with those obtained from an inviscid characteristics program. The experimental boundary-layer data were analyzed by using similarity laws, where the experimental profiles were transformed to the incompressible plane and correlated with the law of the wall. In addition, analytical predictions of laminar-turbulent boundary-layer transition and boundary-layer growth were compared with the inlet test results. The effects of the shock - boundary-layer interactions both with and without bleed were also analyzed and compared with experimental data.

The inlet tests were conducted at the design Mach number of 2.5 and free-stream unit Reynolds numbers of 8.2×10^6 and 2.7×10^6 per meter. This investigation, however, concentrates on the high Reynolds number case. Five bleed configurations were studied, where the total bleed rate varied from 3.6 to 12.7 percent of the total inlet capture mass flow.

SYMBOLS

C_f	skin-friction coefficient
m_b/m_{bl}	ratio of bleed to boundary-layer mass flow
m_b/m_0	ratio of bleed to capture mass flow
P	total pressure, N/m^2; lb/ft^2
p	static pressure, N/m^2; lb/ft^2
R_c	radius of cowl lip, 23.66 cm; 9.315 in.
U	local velocity, m/sec; ft/sec
U_τ	friction velocity, $U_e\sqrt{\frac{C_f}{2}}$, m/sec; ft/sec

x axial distance from centerbody tip, cm; in.

y distance normal to inlet surface, cm; in.

α angular location, deg

δ^* displacement thickness, cm; in.

ζ local Reynolds number based on friction velocity, $\rho_e U_\tau y/\mu_e$

θ momentum thickness, cm; in.

μ viscosity coefficient, (N)(sec)/m^2; (lbf)(sec)/ft^2

ρ local density, kg/m^3; lbm/ft^3

Subscripts:

b bleed

e boundary-layer edge

Superscript:

$\bar{}$ quantities in incompressible plane

DISCUSSION OF ANALYSIS AND DATA

The data used in this investigation were obtained from the Mach 2.50 axisymmetric mixed-compression inlet described in references 3 and 4.

At the design Mach number the inlet had a capture area of 0.1758 square meter and obtained 40 percent of its area contraction externally from a 12.5° half-angle cone centerbody. Coefficients for the equation describing the inlet internal contours are given in table I. The inlet design included porous bleed regions for boundary-layer control. Bleed regions were located to correspond with the cowl and second centerbody oblique-shock impingement points. Additional bleed regions were located in the inlet throat area.

Details of the internal inlet design are shown schematically in figure 1. Both the theoretical and experimental shock locations are shown in the figure. The locations of the bleed regions are measured in terms of the ratio of longitudinal distance from the centerbody tip to the cowl lip radius, x/R_c. The bleed holes were normal to the inlet surface and were 0.3175 centimeter in diameter. The holes were equally spaced around the circumference with alternate rows staggered so that the maximum distance between hole centers for the forward bleed regions was 0.4763 centimeter.

The five bleed hole arrangements tested are listed in table II. In relation to the experimental shock impingement points the bleed arrangement designated US was upstream; AS was across; and DS, DS-I, and DS-III, were downstream. The forward and aft cowl bleed flows were ducted and measured separately, while the centerbody

bleed flows were combined and measured in a single plenum. Translating pitot pressure probes were used to measure the boundary-layer properties at seven locations in the inlet as shown in figure 1. Surface static pressures were measured along the cowl and centerbody surfaces.

The boundary-layer velocity profiles presented in this investigation were calculated from the Mach number profiles of reference 3 by using the Crocco relation between the local boundary-layer velocity and temperature. The velocity profile data were further reduced by using similarity laws. In this case, the method used is that outlined by Baronti and Libby in reference 5. This technique is based on the idea that data in the compressible plane can be transformed to the incompressible plane and subsequently compared with the incompressible form of the law of the wall. The method involves an iteration on the incompressible skin-friction coefficient until the transformed experimental data and the law of the wall in the incompressible plane agree. The value of the incompressible skin-friction coefficient obtained from this correlation is assumed to be correct for that specific set of data. It is then transformed back to the compressible plane, and the compressible skin-friction coefficient is obtained. In addition to providing a direct method for obtaining the surface friction from the data, this method evaluates the validity of individual data points, especially near the wall, where they might be affected by wall interference. This method also indicates any experimentally observed velocity distributions that differ from equilibrium as a result of severe pressure gradients and transverse surface curvature within the inlet. Although the boundary-layer profiles were not measured in the immediate bleed or shock interaction regions, the boundary layers could still be in the process of relaxation following the abrupt change in external or boundary conditions, or both, associated with these situations. Therefore, in cases where the similarity method fails, the boundary layer can be assumed to be badly distorted by the bleed or shock or both.

For a complete boundary-layer analysis on the inlet, a method of estimating the boundary-layer transition locations was necessary. The transition location on the cowl was determined by using the semiempirical method of reference 6. This method is based on data taken in wind tunnels with different turbulence levels, which means the results would represent an average transition location for the given flow condition. The transition location on the conical centerbody was estimated by a two-step procedure. First, a flat-plate transition location was determined by using the centerbody tip bluntness and local flow conditions on the surface. Second, the ratio of transition between a cone and a flat plate was estimated from reference 7, which presents an experimental comparison of the transition between a sharp tipped cone and a hollow cylinder. From these values the transition location on the centerbody was then determined.

A finite-difference boundary-layer technique described in reference 8 was used to calculate both the laminar and turbulent boundary-layer properties along the internal inlet surfaces. However, for these calculations the turbulence model was not modified

for the nonequilibrium boundary-layer regions in the vicinity of transition and the shock interactions. The boundary-layer calculation was terminated upstream of each interaction region, and a separate analysis was then used to determine the boundary-layer properties downstream of the interaction. The boundary-layer program was then restarted by using these properties. The calculated inviscid static-pressure distribution was used in these calculations. No attempt was made to calculate boundary-layer properties downstream of probe 3 because the exact structure involving the oblique and terminal shocks was not known. Therefore, there was no comparison of analytical and experimental results downstream of the terminal shock.

Determining the change in boundary-layer properties across the shock interaction regions involved the study of two kinds of shock - boundary-layer interactions, without and with bleed. Those that occurred on the forward centerbody were without bleed, while those on the cowl were with bleed, at rather high bleed rates in the interaction region. For the interactions with bleed, the integral control volume technique of Seebaugh, Paynter, and Childs in reference 9 was used. This method uses a model having three alternative bleed devices - a porous wall, a flush slot, and a scoop. The porous-wall model, which assumes no streamwise momentum leaving with the bleed flow, overestimated the observed effectiveness of the bleed, and no solution was possible for the values of bleed flow rates used in the inlet tests. The flush-slot model, which assumes the bleed flow leaves the control volume with the same momentum it has entering the control volume, also failed to give a solution for the boundary-layer and bleed conditions of the inlet tests. The ram scoop model assumes the bleed leaves the control volume with its total momentum, including its incoming pressure-area term. It is suggested in reference 10 that the scoop model of reference 9 is also applicable to flush-bleed situations. In the appendix it is shown that the scoop-bleed model is equivalent to a plausible flush bleed model if the pressure along the dividing streamline between the bleed flow and the residual layer is assumed equal to the edge pressure of the control volume. Therefore, this model was used in the analysis of the interactions having bleed.

Although the control volume analysis of reference 9 is applicable to interactions without bleed, no solution was possible for the boundary-layer conditions and shock strength on the forward centerbody. As reported in reference 3, the boundary layer did have a substantial separated region at this interaction for the low Reynolds number tests. This, along with comparing the pressure rise across the interaction to that predicted for incipient separation in reference 11, indicated a possible separation also existed in the interaction region for the high Reynolds number case under consideration in this report. Therefore, the semiempirical method of Pinckney in reference 12 was used for this interaction. The model in this method is compatible with the existence of a separated region.

RESULTS AND DISCUSSION

The data analyzed in this investigation involve the series of tests initially presented in reference 3 for a free-stream Reynolds number of 8.2×10^6 per meter and the inlet operating in mode C, where the shock is located in the throat region. In table III the boundary layer integral thicknesses, along with the bleed rates, are presented. In figure 2 the velocity profiles that have been transformed by the method of Baronti and Libby (ref. 5) are presented along with the law of the wall profiles. The profiles for probes 1, 2, 3, and 5, which are essentially unaffected by the change in bleed configurations, are presented only once. In figure 2(a), which applies for all bleed configurations, the profiles show good agreement with the law of the wall over most of the range of expected correlation. The good agreement of probes 1, 3, and 5 would be expected since the boundary layer at these locations had not experienced any shock interactions or in the case of probe 3 had sufficient time to recover The remaining profiles in figures 2(b) to (f) show the results for the various bleed configurations. The agreement is acceptable for most profiles with the obvious exception of probe 7 for the US and AS bleed configurations. Since probe 7 was located in the vicinity of the terminal shock, this indicates the boundary layer was distorted at this location for those two bleed configurations. For the three DS bleed configurations, where the bleed regions were located farther aft, the boundary layers were closer to equilibrium. In addition, for several of the profiles the data points nearest the wall did not agree with the theory; this could have been a result of interference between the probe and the wall. In table IV the skin-friction coefficients obtained from the law of the wall correlation are given along with those predicted by the method of Spalding and Chi (ref. 13). The two values of the skin-friction coefficients obtained from the profiles for which the law of the wall correlation was unsatisfactory are noted in the table.

The comparison of an experimental and calculated static-pressure distribution is shown in figure 3. The theoretical values are obtained from the inviscid characteristics program of reference 14. These values agree with the data up to the location where the bleed regions and terminal shock began to influence the pressure distribution.

Figure 4 presents the comparison of experimental and calculated displacement and momentum thicknesses on the centerbody for the various bleed configurations. The theoretical curve represents values obtained with the transition location estimated at 38.4 centimeters by the previously discussed technique. The location of transition was not measured directly, so the prediction method must be evaluated indirectly by determining the accuracy with which the integral parameters were calculated at the first boundary-layer probe on the centerbody. From these results, shown in figure 4, it appears the transition prediction was reasonably accurate. Farther downstream at probes 2 and 3, which are located behind the first shock interaction and upstream of the forward centerbody bleed region, respectively, the calculated parameters were higher than the

data. Most of this inaccuracy results from an accumulation of errors starting with a slight overprediction of the boundary-layer parameters at the first probe, which could have resulted from predicting transition prematurely. In addition, the method of reference 12, used for the shock - boundary-layer interaction, gave somewhat higher thickness values than those measured across the interaction.

A similar comparison between experimental and calculated boundary-layer parameters is presented for the cowl in figure 5. The boundary-layer transition location was estimated from reference 6 at 12.5 centimeters from the cowl leading edge. The comparison of the results at probe 5 indicates this estimate was accurate. At probe 6, which is downstream of the interaction and bleed region, the results show relatively good agreement between the calculated and experimental values for most bleed cases. The poorest agreement occurs for the US bleed case, while the most accurate is the AS bleed case. These results might be explained by the characteristics of the model used for the interaction analysis, where the bleed is assumed to be taken out in the interaction region. This assumption would be most nearly correct for the AS case and farthest from the actual conditions for the US case, where the bleed extends some distance upstream of the interaction region.

In figure 6 the calculated boundary-layer velocity profiles from the method of reference 8 are compared with the experimental profiles for probes 1, 2, 3, and 5. These profiles are unaffected by the bleed and apply for all bleed cases. The agreement is good for all probes except 3, where the experimental profile is fuller than the calculated. The calculated and experimental profiles for probe 6, which is downstream of the cowl interaction and bleed region, are presented in figure 7. The agreement of these profiles was not as good as that of those upstream of the interaction and bleed. Again, as in the comparison of the integral parameters, the US case showed the poorest agreement because the assumptions in the interaction analysis were farthest from the actual bleed conditions.

The boundary-layer calculations were performed by using the theoretical static-pressure distribution. As shown in figure 3, the theoretical and experimental pressure distributions were in disagreement for the aft portion of the inlet, which could account for some of the discrepancies between the experimental and calculated boundary-layer parameters. Somewhat better agreement might be obtained by using the experimental pressure distribution or performing an iteration between the boundary-layer results and the inviscid characteristics program.

SUMMARY OF RESULTS

An analytical investigation was made of the boundary-layer flow in an axisymmetric mixed-compression inlet, and the results were compared with experimental measure-

ments. The inlet under study was designed for operation at Mach number 2.5 and utilized a bleed system for boundary-layer control. The experimental measurements included internal surface static pressures and pitot pressure surveys through the boundary layers both upstream and downstream of the shock - boundary-layer interactions. The surface static pressures were compared with those obtained from an inviscid characteristics program. Boundary-layer analyses were used that predicted laminar and turbulent boundary-layer growth, transition, and the effects of the shock - boundary-layer interactions. These interactions were both with and without bleed in the interaction region. From these studies the following results were obtained:

1. The boundary-layer transition was estimated satisfactorily on the cowl by using a semiempirical flat-plate prediction technique and on the centerbody by modifying this technique for conical flow.

2. A finite-difference boundary-layer program was used with satisfactory results to predict both laminar and turbulent boundary-layer characteristics.

3. Good agreement was obtained between the analysis and data for the change in cowl boundary-layer properties across the shock interaction with bleed by using an integral control volume technique. The integral control volume technique gave the best results for the case that compared most nearly to the conditions of the analytical model, that is, where the bleed was removed in the interaction region.

4. For the shock - boundary-layer interaction without bleed, where a separation may have been present, the integral control volume technique was not satisfactory. A semiempirical method that is compatible with the existence of a separation was used with substantially better results.

5. Disagreement between theoretical and experimental pressure distributions for the aft portion of the inlet probably contributed to discrepancies between experimental and calculated boundary-layer parameters.

6. The inviscid characteristics program was able to predict accurately the internal static-pressure distribution up to an axial location in the vicinity of the shock impingement point on the cowl.

Lewis Research Center,
National Aeronautics and Space Administration,
Cleveland, Ohio, December 12, 1973,
501-24.

APPENDIX - COMPARISON OF SCOOP AND DIVIDING STREAMLINE MODELS

As stated previously, Green in reference 10 suggested that the scoop bleed model of Seebaugh, Paynter, and Childs in reference 9 might be used for other bleed configurations. It can be shown that this scoop model is numerically equivalent to a plausible flush bleed model. The continuity equation for the scoop model shown in figure 8(a) is written as

$$\left(1 - \frac{m_b}{m_{bl}}\right)\rho_{e1}u_{e1}\int_0^{\delta_1}\frac{\rho u}{\rho_e u_e}\,dy\Big|_1 = \rho_{e_3}u_{e_3}\int_0^{\delta_3}\frac{\rho u}{\rho_e u_e}\,dy'\Big|_3 \tag{1}$$

and the momentum equation is stated as

$$p_1(\delta_1 - y_s) - p_2(\delta_1 - \delta_3 - y_3) - p_3\delta_3 = \int_0^{\delta_3}\rho u^2\,dy'\Big|_3 - \int_{y_s}^{\delta_1}\rho u^2\,dy\Big|_1 \tag{2}$$

The dividing streamline model shown in figure 8(b) differs from the scoop model in that the lower surface of the control volume is not a solid surface but a streamline described by the fluid particle that enters the bleed system farthest downstream. If the average pressure along this streamline is taken as p_4 and the momentum flux across this streamline is assumed to be negligible, which is consistent with the assumption of negligible skin friction in the interaction region of the scoop model, the continuity and momentum equations for the dividing streamline model can be written as

$$\left(1 - \frac{m_b}{m_{bl}}\right)\rho_{e1}u_{e1}\int_0^{\delta_1}\frac{\rho u}{\rho_e u_e}\,dy\Big|_1 = \rho_{e_3}u_{e_3}\int_0^{\delta_2}\frac{\rho u}{\rho_e u_e}\,dy\Big|_3 \tag{3}$$

and

$$p_1(\delta_1 - y_s) + p_4 y_s - p_2(\delta_1 - \delta_3) - p_3\delta_3 = \int_0^{\delta_3}\rho u^2\,dy\Big|_3 - \int_{y_s}^{\delta_1}\rho u^2\,dy\Big|_1 \tag{4}$$

Equation (3) is identical to (1) with the exception that the integral at station 3 is evaluated with respect to y rather than y'. In addition, if the pressure along the dividing

streamline p_4 is assumed to be equal to p_2, equation (4) becomes

$$p_1(\delta_1 - y_s) - p_2(\delta_1 - \delta_3 - y_3) - p_3\delta_3 = \int_0^{\delta_3} \rho u^2 \, dy\Big|_3 - \int_{y_s}^{\delta_1} \rho u^2 \, dy\Big|_1 \qquad (5)$$

Again with the exception of the integral at station 3 being evaluated with respect to y, equation (5) is identical to equation (2). Therefore, the scoop model is equivalent to the flush bleed dividing streamline model if it is kept in mind that the thicknesses at station 3 are measured from the original surface and not y_s.

REFERENCES

1. Smeltzer, Donald B.; and Sorensen, Norman E.: Analytic and Experimental Performance of Two Isentropic Mixed Compression Axisymmetric Inlets at Mach Numbers 0.8 to 2.65. NASA TN D-7320, 1973.

2. Reyhner, Theodore A.; and Hickcox, Timothy E.: Combined Viscous-Inviscid Analysis of Supersonic Inlet Flowfields. J. Aircraft, vol. 9, no. 8, Aug. 1972, pp. 589-595.

3. Hingst, Warren R.; and Johnson, David F: Experimental Investigation of Boundary Layers in an Axisymmetric, Mach 2.5, Mixed-Compression Inlet. NASA TM X-2902, 1973.

4. Cubbison, Robert W.; Meleason, Edward T.; and Johnson, David F.: Effect of Porous Bleed in a High-Performance Axisymmetric, Mixed-Compression Inlet at Mach 2.50. NASA TM X-1692, 1968.

5. Baronti, Paolo O.; and Libby, Paul A.: Velocity Profiles in Turbulent Compressible Boundary Layers. AIAA J., vol. 4, no. 2, Feb. 1966, pp. 193-202.

6. Hopkins, Edward J.; Jillie, Don W.; and Sorensen, Virginia L.: Charts for Estimating Boundary-Layer Transition on Flat Plates. NASA TN D-5846, 1970.

7. Brinich, Paul F.: Boundary-Layer Transition on an Open-Nose Cone at Mach 3.1. NACA TN 4214, 1958.

8. McDonald, H.; and Fish, R. W.: Practical Calculations of Transitional Boundary Layers. Int. J. Heat Mass Transfer, vol. 16, no. 9, Sept. 1973, pp. 1729-1744.

9. Seebaugh, William R.; Paynter, Gerald C.; and Childs, Morris E.: Shock-Reflection from a Turbulent Boundary Layer with Mass Bleed. J Aircraft, vol. 5, no. 5, Sept.-Oct. 1968, pp. 461-467.

10. Green, J. E.: Interactions Between Shock Waves and Turbulent Boundary Layers. Rep. RAE-TR-69098, Royal Aircraft Establishment, May 1969.

11. Kuehn, Donald M.: Experimental Investigation of the Pressure Rise Required for the Incipient Separation of Turbulent Boundary Layers in Two-Dimensional Supersonic Flow. NASA Memo 1-21-59A, 1959.

12. Pinckney, S. Z.: Semiempirical Method for Predicting Effects of Incident-Reflecting Shocks on the Turbulent Boundary Layer. NASA TN D-3029, 1965.

13. Spalding, D. B.; and Chi, S. W: The Drag of a Compressible Turbulent Boundary Layer on a Smooth Flat Plate with and without Heat Transfer. J. Fluid Mech., vol. 18, Jan. 1964, pp. 117-143.

14. Anderson, Bernhard H.: Design of Supersonic Inlets by a Computer Program Incorporating the Method of Characteristics. NASA TN D-4960, 1969.

TABLE I - COEFFICIENTS FOR INLET CONTOUR EQUATION

[Radius of body $r = a_0 + a_1(x/R_c) + a_2(x/R_c)^2 + a_3(x/R_c)^3$.]

Coefficient				
a_0	a_1	a_2	a_3	min x/R_c
Centerbody				
0	0. 221690	0	0	0
- 117562	- 0686815	244819	- 0450772	2. 87348
-80. 1714	67 6828	-18 8490	1 74666	3. 43532
9. 05786	-6. 37110	1 63555	- 141953	3. 65003
- 549874	972234	- 232649	016264	4. 37944
-1 00723	1 11977	- 233621	0141971	4. 72356
Cowl				
1 000	0	0	0	2. 00852
632074	335405	- 0876992	00493565	2. 39748
791069	214535	- 0612318	00366218	2. 88342
6. 34488	-4. 24523	1 12573	- 100948	3. 54267
7 37531	-4. 55285	1. 07795	- 0858415	3. 86473
2. 35019	- 869625	178072	- 0125569	4. 07944
1 34645	-8 20127	1. 78457	- 0129433	4. 29415
- 0518106	641500	- 0143778	0107363	4. 56253

TABLE II. - LOCATIONS OF INLET POROUS BLEED CONFIGURATIONS

[Row open, ○, row closed, ●, and row with alternate holes closed, ◑.]

Configuration	Cowl bleed		Centerbody bleed
	Forward	Aft	
US	○○○○○○●●●●●●	◑● ●●	○○○●●●●●◑●◑◑ ◑ ●
AS	●●●●○○○●●●●●	◑● ◑●	●◑○○○◑●●●◑◑◑◑ ◑ ●
DS	●●●●●●○○●●●●	◑● ◑●	●●●○○○◑●●◑◑◑◑ ◑ ●
DS-I	●●●●●●○○●●●●	●● ●●	●●●○○○◑●● ● ● ● ● ●
DS-III	●●●●●●○○○○○○	○○ ○○	●●●○○○○○○ ○ ○ ○ ○ ○

TABLE III. - EXPERIMENTAL BLEED RATES AND BOUNDARY-LAYER INTEGRAL THICKNESSES

Bleed configuration	Bleed rate parameter				Probe	Displacement thickness, δ^*, cm	Momentum thickness, θ, cm
	Forward m_b/m_0 on cowl	Forward m_b/m_{bl} on cowl	m_b/m_0 On centerbody	Forward m_b/m_0 on centerbody			
DS	0.0155	0.283	0.0295	0.0207	1	0.1134	0.0313
					2	1432	0495
					3	1141	0452
					4	1218	0612
					5	0811	0298
					6	0750	0358
					7	1238	0600
DS-1	0.0153	0.280	0.0207	0.0207	1	0.1145	0.0334
					2	1342	0485
					3	1170	0483
					4	1261	0627
					5	0784	0287
					6	0741	0362
					7	1327	0626
US	0.0213	0.390	0.0314	0.0182	1	0 1147	0.0333
					2	1133	0386
					3	1179	0481
					4	1357	0789
					5	0836	0313
					6	0795	0395
					7	0881	0486
AS	0.0179	0.329	0.0329	0.0154	1	0.1015	0.0295
					2	1192	0429
					3	1097	0450
					4	1721	0920
					5	0844	0314
					6	0532	0264
					7	0865	0455
DS-III	0.0336	0.615	0.0556	0.0052	1	0.1094	0.0304
					2	1271	0435
					3	1174	0453
					4	1169	0540
					5	0789	0291
					6	0289	0134
					7	0428	0202

TABLE IV - SKIN-FRICTION COEFFICIENTS OBTAINED FROM SIMILARITY TECHNIQUE COMPARED WITH METHOD OF REFERENCE 13

Bleed configuration	Probe	Skin-friction coefficient	
		Similarity technique	Method of ref. 3
US	1	0.00277	0.00231
	2	00202	00256
	3	00253	00266
	4	00245	00266
	5	00287	00279
	6	00275	00286
	7	[a] 00180	00267
AS	4	0.00229	0.00268
	6	00286	00286
	7	[a] 00177	00266
DS	4	0.00276	0.00258
	6	00253	00292
	7	00278	00278
DS-I	4	0.00255	0.00241
	6	00325	00302
	7	00282	00279
DS-III	4	0.00236	0.00266
	6	00384	00351
	7	00347	00317

[a]Obtained from profiles for which law of the wall correlation was unsatisfactory

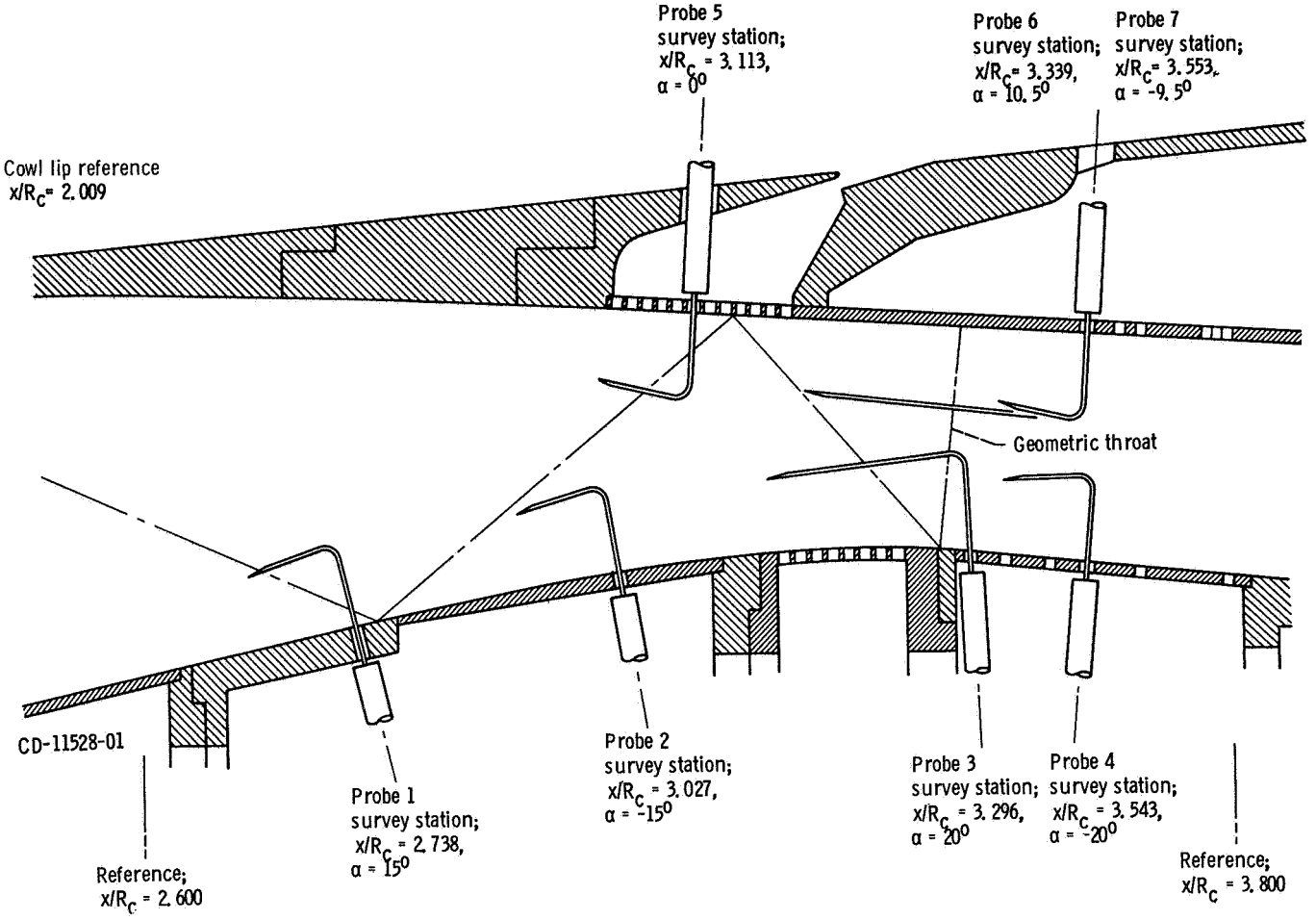

Figure 1. - Location of boundary-layer probes on inlet model. Axial distance, x/R_C; angular location of probe, α, measured clockwise from bottom vertical centerline looking downstream.

Theory
Experimental data
Probe
1
2
22
18
14
10
6
2
26
22
18
14
10
6
2
to transformed friction velocity, $\bar{U}/\bar{U}_t$

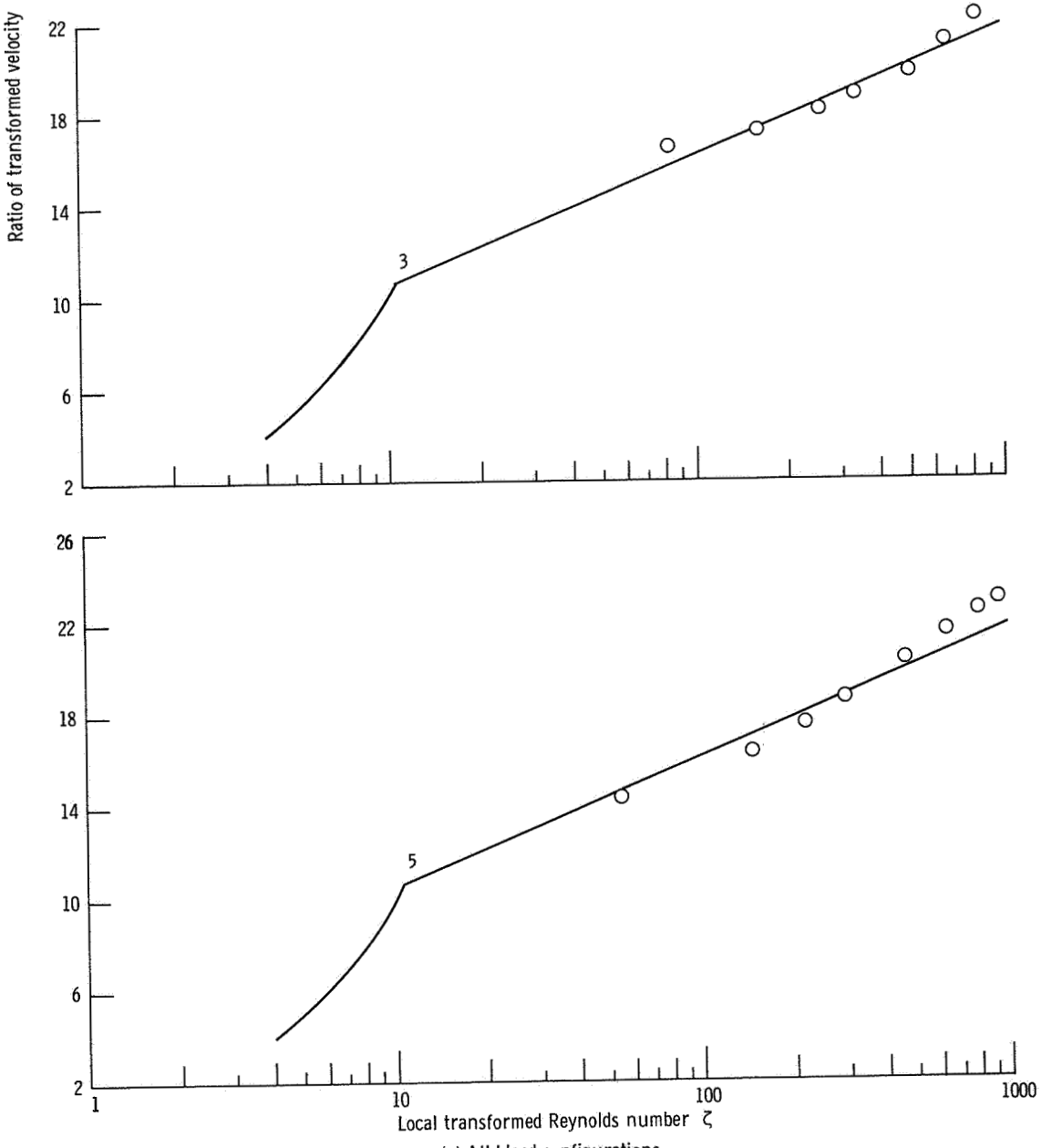

(a) All bleed configurations.

Figure 2. Velocity profiles.

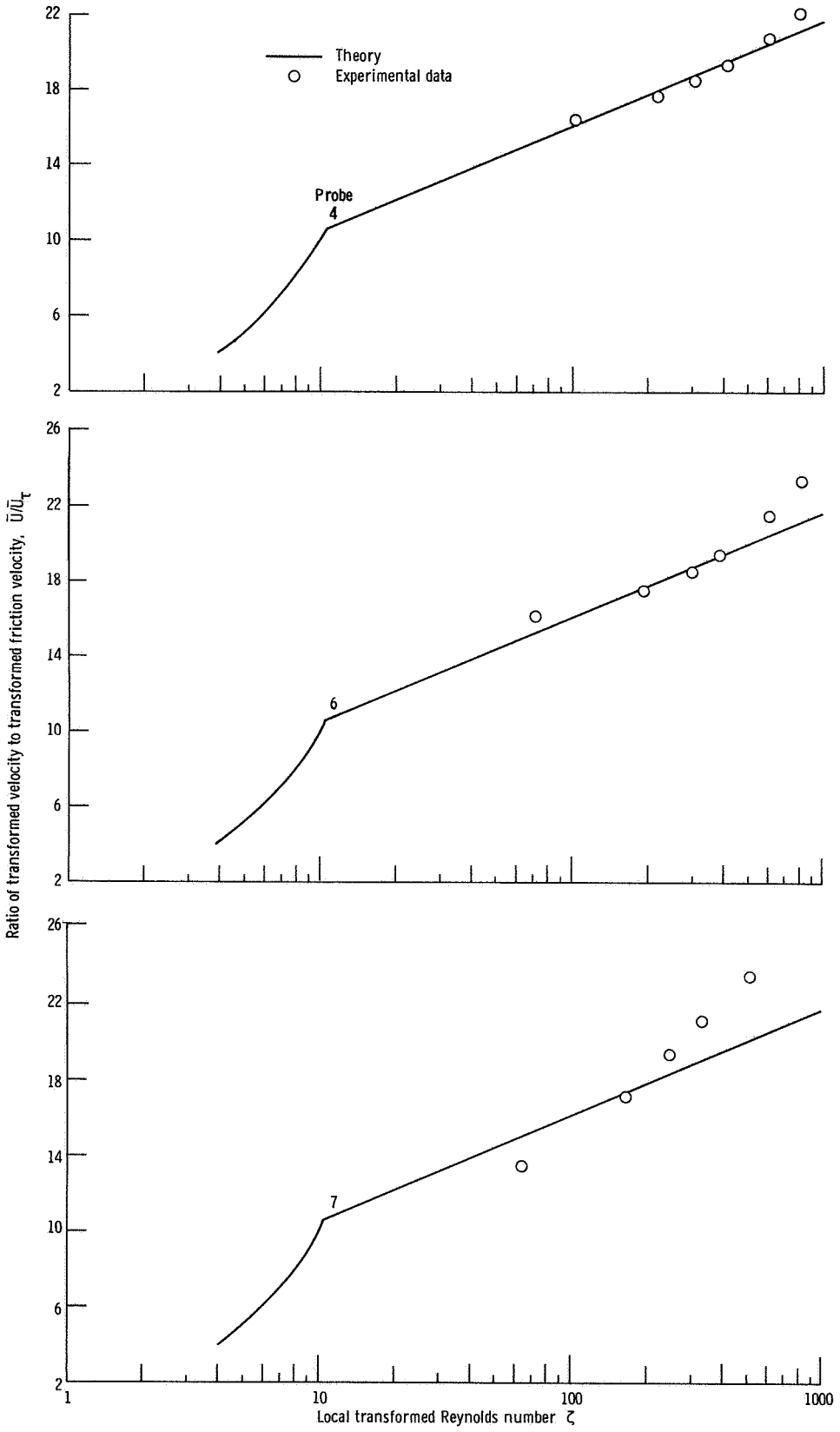

(b) US bleed configuration.

Figure 2. Continued.

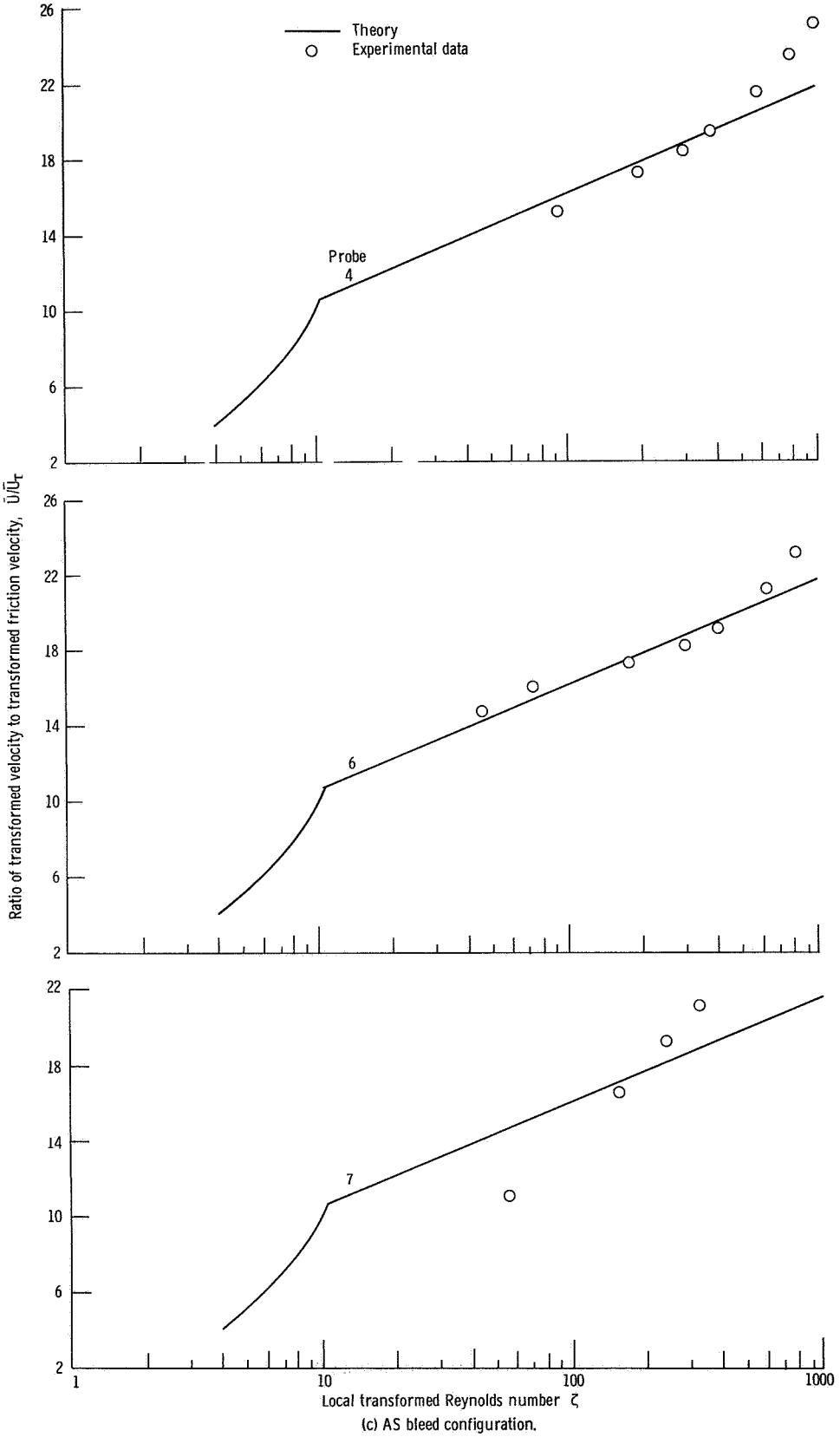

(c) AS bleed configuration.

Figure 2. Continued.

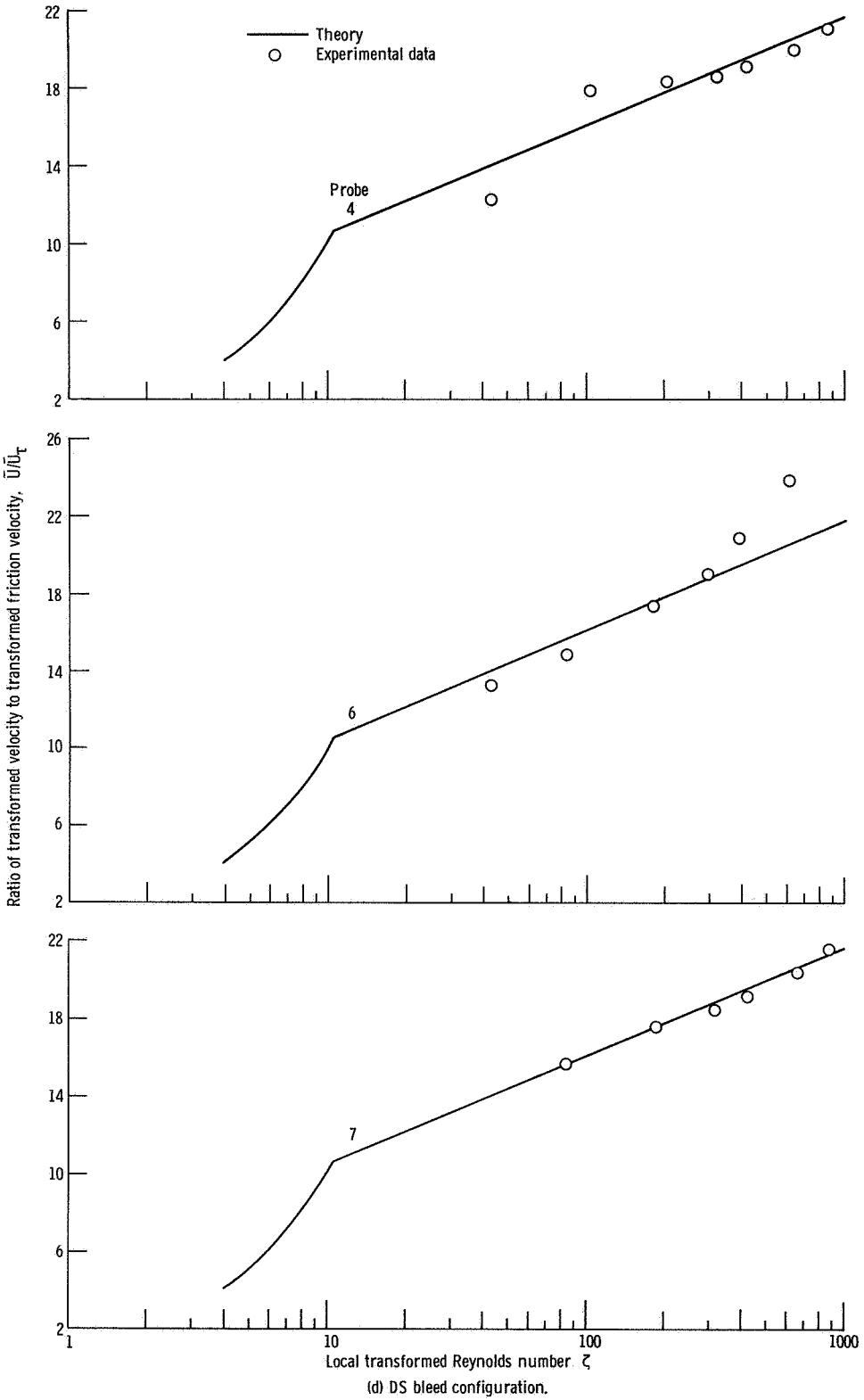

(d) DS bleed configuration.

Figure 2. Continued.

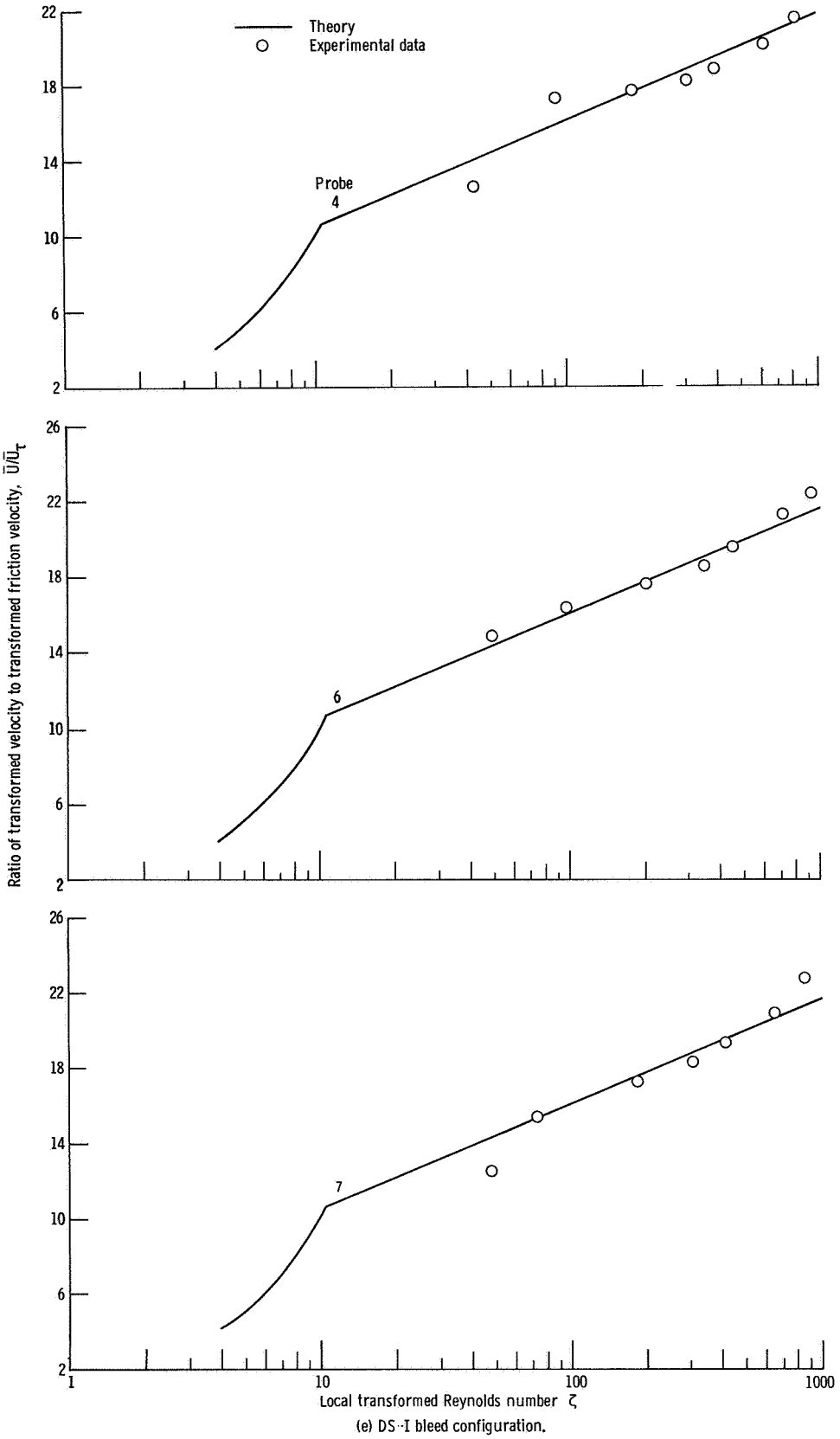

(e) DS-I bleed configuration.

Figure 2. Continued.

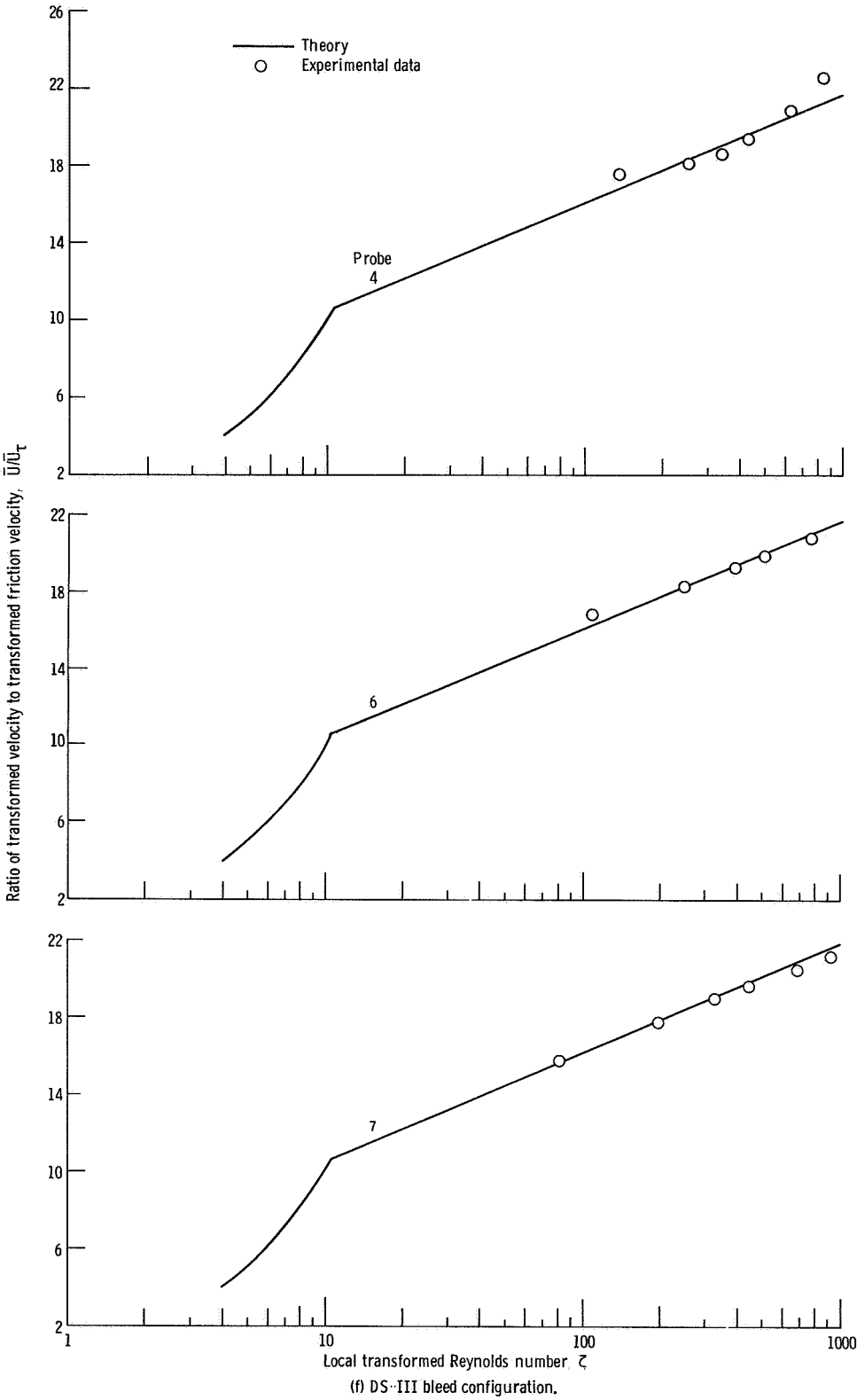

(f) DS-III bleed configuration.

Figure 2. Concluded.

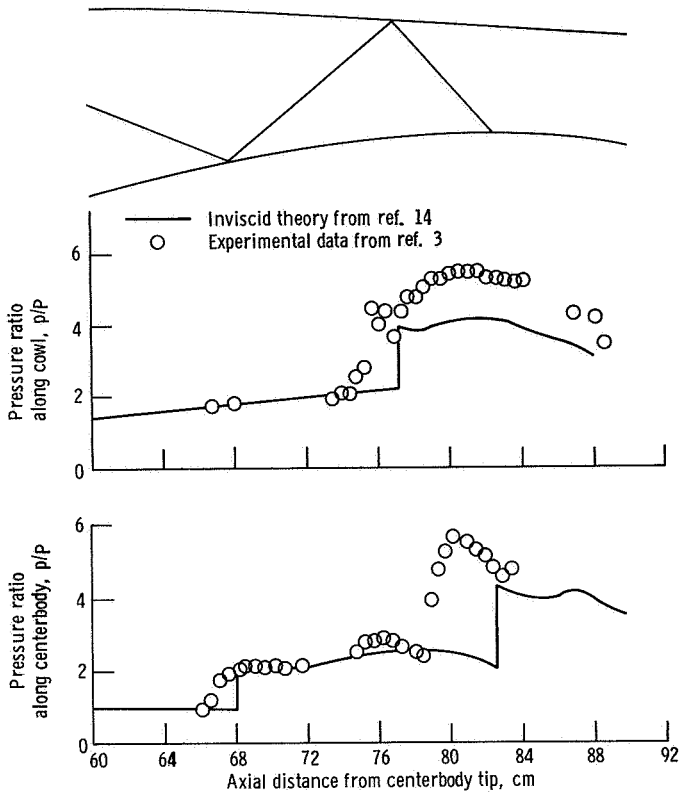

Figure 3. Theoretical and experimental pressure distribution for US bleed configuration.

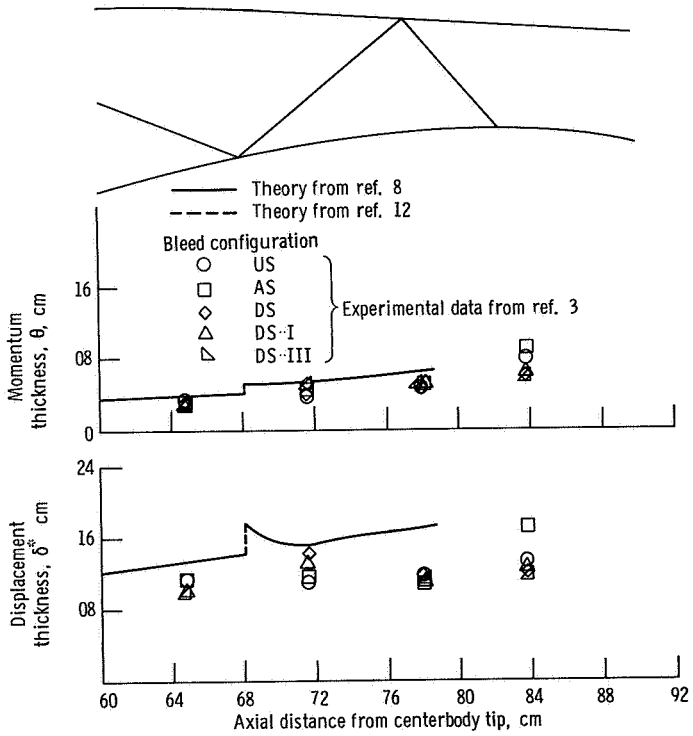

Figure 4. Theoretical and experimental boundary-layer parameters along centerbody for all bleed configurations.

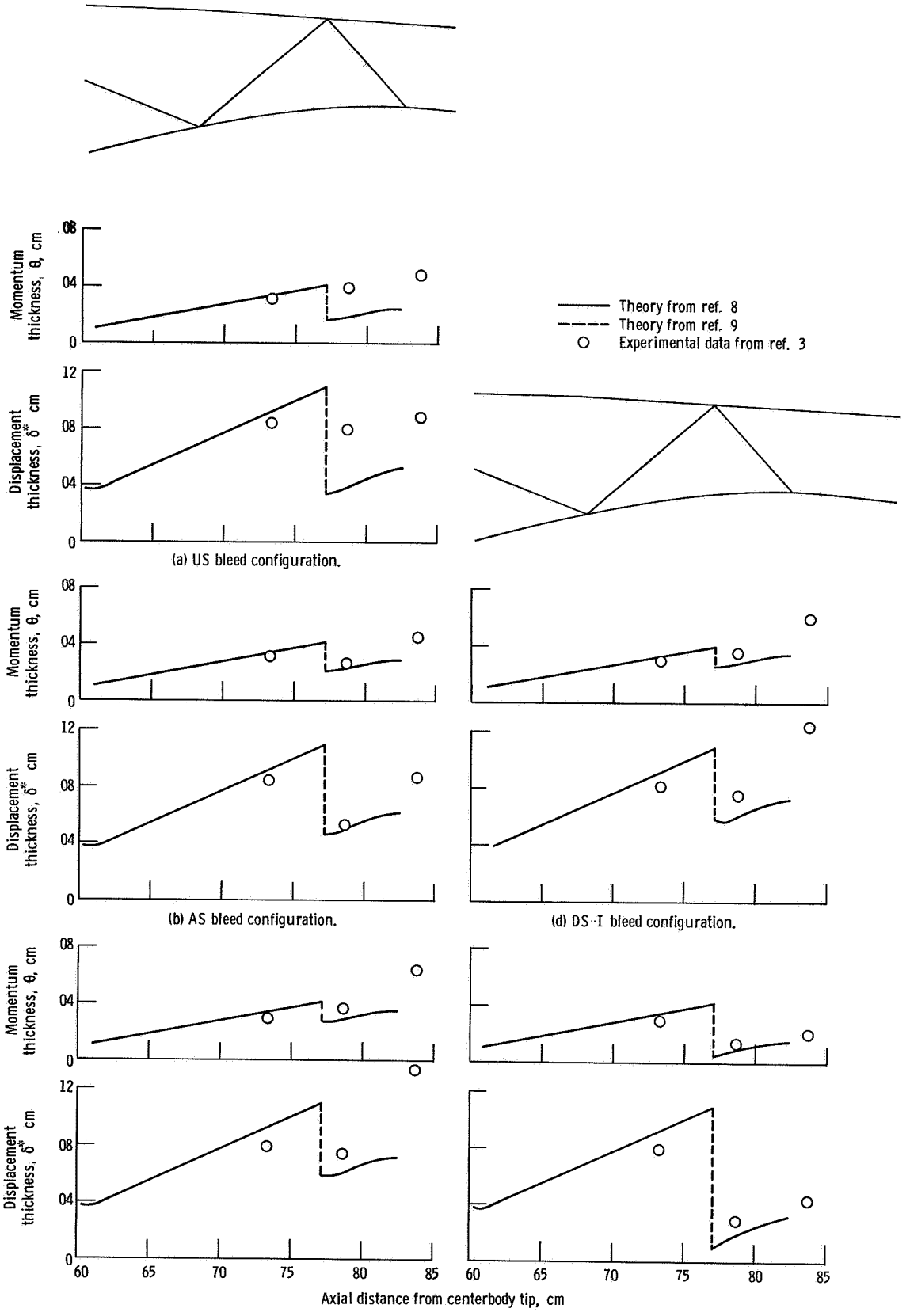

Figure 5. Theoretical and experimental boundary-layer parameters along cowl.

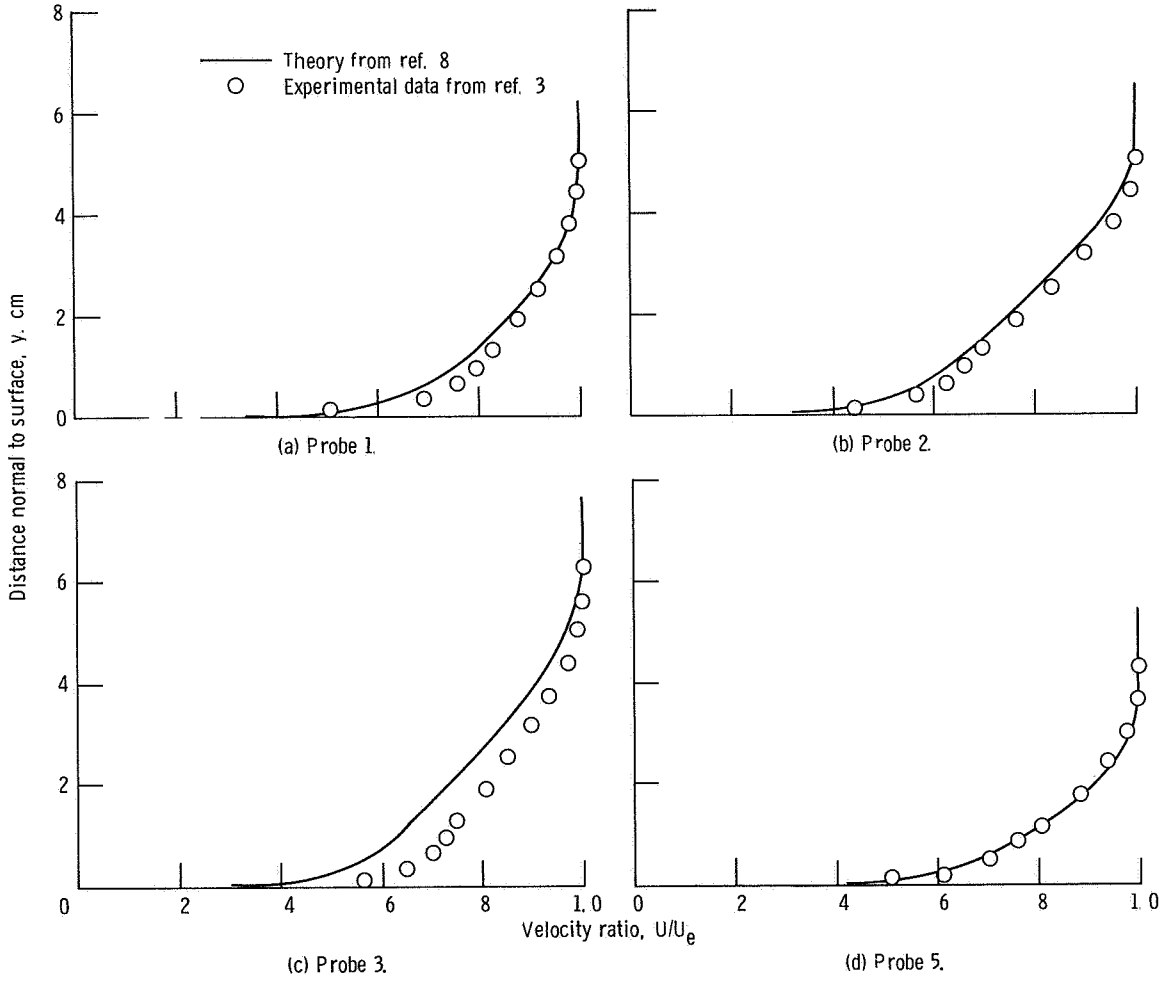

Figure 6. Comparison of experimental and calculated boundary-layer profiles for all bleed configurations.

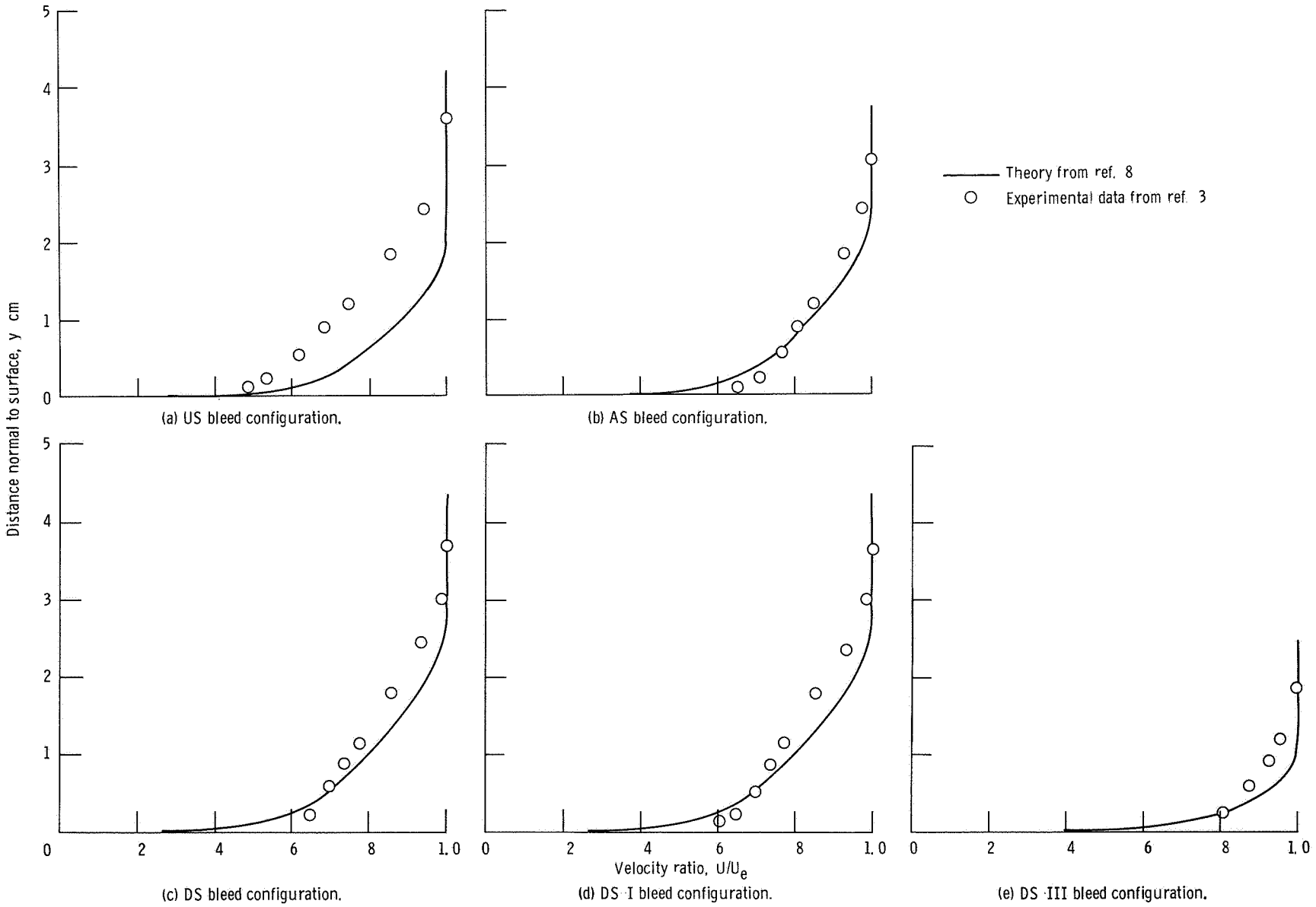

Figure 7. Comparison of experimental and calculated boundary-layer profiles at probe 6 for various bleed configurations.

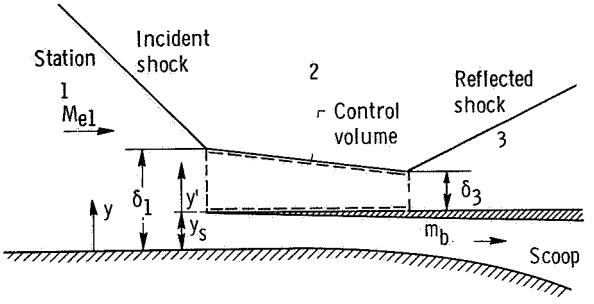

(a) Scoop suction model.

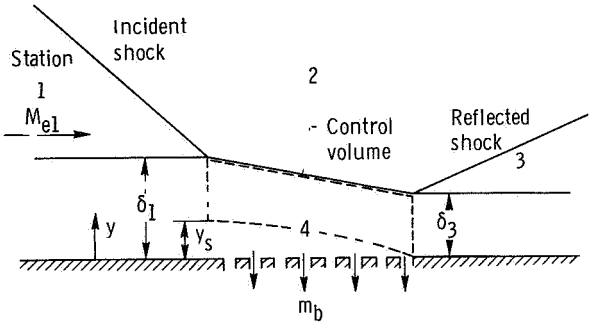

(b) Dividing streamline model.

Figure 8. Control volumes for shock boundary-layer interaction models.